Probing the dynamics of dissociation of methane following core ionization using three-dimensional molecular-frame photoelectron angular distributions

2012 J. Phys. B: At. Mol. Opt. Phys. 45 194003

(http://iopscience.iop.org/0953-4075/45/19/194003)

J. Phys. B: At. Mol. Opt. Phys. **45** (2012) 194003 (10pp) doi:10.1088/0953-4075/45/19/194003

Probing the dynamics of dissociation of methane following core ionization using three-dimensional molecular-frame photoelectron angular distributions

J B Williams[1], C S Trevisan[2], M S Schöffler[3], T Jahnke[3], I Bocharova[4], H Kim[3], B Ulrich[3], R Wallauer[3], F Sturm[3], T N Rescigno[4], A Belkacem[4], R Dörner[3], Th Weber[4], C W McCurdy[4,5] and A L Landers[1]

[1] Department of Physics, Auburn University, Auburn, AL 36849, USA
[2] Department of Sciences and Mathematics, California Maritime Academy, Vallejo, CA 94590, USA
[3] Institut für Kernphysik, J W Goethe Universität, Max-von-Laue-Str. 1, Frankfurt 60438, Germany
[4] Lawrence Berkeley National Laboratory, Chemical Sciences, Berkeley, CA 94720, USA
[5] Department of Chemistry, University of California, Davis, CA 95616, USA

E-mail: LANDEAL@auburn.edu

Received 14 March 2012, in final form 17 May 2012
Published 24 September 2012
Online at stacks.iop.org/JPhysB/45/194003

Abstract
We present experimental measurements and theoretical calculations for the photoionization of CH_4 at the carbon K-edge. Measurements performed using cold target recoil ion momentum spectroscopy (COLTRIMS) combined with complex Kohn variational calculations of the photoelectron in the molecular frame demonstrate the surprising result that the low energy photoelectrons effectively image the molecule by emerging along the bond axes. Furthermore, we observe a dynamic breakdown of axial recoil behaviour in one of the dissociation pathways of the intermediate dication, which we interpret using electronic structure calculations.

(Some figures may appear in colour only in the online journal)

1. Introduction

The measurement of molecular-frame photoelectron angular distributions (MFPADs) promises to become a general technique to probe molecular and electronic dynamics in ultrafast experiments. It is important therefore to develop an understanding of the various ways in which MFPADs can be sensitive to both a molecule's structure and its electronic state. Both theoretical and experimental studies are exploring this question [1, 2], and recently the present authors observed [3] that in some cases the MFPAD for core electron photoejection, averaged over all photon polarizations, can effectively image the geometry of a polyatomic molecule in three dimensions, with the outgoing electron effectively focused along the bond directions.

In this study we pursue the question of how the measurement of three-dimensional MFPADs for polyatomic molecules in momentum imaging experiments can reveal aspects of molecular dynamics when the photoionization event is followed by dissociation of the molecule. To measure an MFPAD, the gas phase molecule must be oriented accurately in the lab frame. Such orientation can be accomplished prior to the ionization by laser alignment [4, 5]. The orientation of the molecule at the time of photoionization can also be determined in the case of core or inner shell ionization by detecting the photoelectron in coincidence with positively charged fragments that emerge following prompt Auger decay and dissociation of the molecule [6]. For polyatomic molecules the complete determination of molecular orientation has recently allowed the measurement of three-dimensional MFPADs in the cases of water [7] and methane [3].

The methane molecule has tetrahedral symmetry and therefore has four equivalent threefold (C_3) axes of symmetry and three equivalent twofold (C_2) axes, as shown in

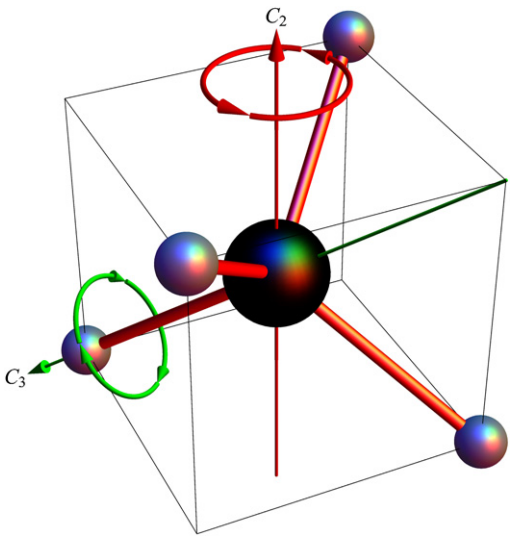

Figure 1. Rotational symmetry axes of methane in tetrahedral symmetry (T_d point group) showing one of three equivalent C_2 axes of symmetry with the red arrow and one of four equivalent C_3 axes with the green arrow.

figure 1. If subsequent to Auger decay it dissociates into two fragments, the molecule's three-dimensional orientation cannot be determined and the observed MFPAD will be averaged over rotation around one of those symmetry axes. In the case of the core ionization of methane (as well as water [7]), the determination of the three-dimensional orientation of the molecule has been greatly aided by the presence of direct double Auger decay that forms a triply charged cation within a few femtoseconds of the primary ionization event, and the subsequent prompt dissociation of the molecule into *three* charged fragments:

$$\begin{aligned} CH_4 + h\nu &\rightarrow CH_4^+(1s^{-1}) + e^- \\ CH_4^+(1s^{-1}) &\rightarrow CH_2^+ + H^+ + H^+ + 2e^-. \end{aligned} \quad (1)$$

The observation of three ionic fragments in coincidence with the photoelectron using the cold target ion momentum spectroscopy (COLTRIMS) method [8, 9] can then yield the complete angular dependence of photoejection in the molecular frame.

However, the single Auger decay process, which in this case can yield other ionic dissociation channels,

$$\begin{aligned} CH_4^+(1s^{-1}) &\rightarrow CH_2 + H^+ + H^+ + e^- \\ &\rightarrow CH_3^+ + H^+ + e^- \\ &\rightarrow CH_2^+ + H_2^+ + e^- \end{aligned} \quad (2)$$

etc, can also yield MFPADs as well as information about the dynamics of these dissociation pathways, even though the last two of these dissociation channels can only yield the MFPADs averaged around the recoil axis. Such measurements are sometimes called recoil-frame photoelectron angular distributions (RFPADs) to distinguish them from the full MFPAD for the completely oriented molecule. These decay channels and many others have been studied before in experiments that observe the Auger electron in coincidence with the ionic fragments [10–12]. In this study we build particularly on the previous work of Kukk *et al* [10] as we focus here on the $[CH_2, H^+, H^+]$ and $[CH_3^+, H^+]$ dissociation channels.

The central question that determines if coincidence measurements in these channels yield information on the orientation of the molecule is whether or not the dissociation dynamics are prompt and the fragmentation occurs essentially along the directions of the bonds in the molecule. This condition, called 'axial recoil' for diatomics may or may not be satisfied because the molecule can rotate before dissociating in some cases [13]. Polyatomic molecules can bend or rearrange bonds during dissociation, and such dynamics have been seen in COLTRIMS and other momentum imaging measurements [14–16]. Thus, polyatomic molecules have many more ways to fail the test of prompt and direct dissociation along the bonds being ruptured. Even in those cases, however, COLTRIMS measurements of the apparent MFPADs, combined with their theoretical prediction, can help elucidate the mechanisms of ionic dissociation.

In this work we demonstrate that the first of the two dissociation channels in equation (2) satisfies the condition of prompt direct dissociation, and thus provides a path to measuring MFPADs in three dimensions in high resolution. The second channel in equation (2) displays direct dissociation along a bond at some values of the kinetic energy release (kinetic energy of the fragments in the centre of mass frame of the molecule) but not at others. If the condition of axial recoil is satisfied by the dynamics, the measured RFPAD should be equivalent to the MFPAD averaged around one of the symmetry axes in figure 1, but not if there is a breakdown of axial recoil. As a result, the combination of experimental observations of the apparent RFPAD in that channel and the measured MFPADs in other channels—together with theoretical calculations using the complex Kohn variational method and quantum chemical calculations of the potential curves for dissociation of CH_4^{++} in various electronic states—yields strong evidence for how the dissociation in that channel occurs and which electronic states are involved.

2. Measurement of MFPADs for methane using the COLTRIMS method

The experiments were performed at the Lawrence Berkeley National Laboratory Advanced Light Source's beam line 11.0.2 using COLTRIMS [6, 8]. A beam of linearly polarized 295 or 306 eV photons from the Advanced Light Source intersected a supersonic gas jet of methane molecules providing measurements of the MFPADs and RFPADs at two electron ejection energies. Because of the cooling through expansion of the jet, the methane target molecules were in the ground vibrational and rotational states. The majority of those molecules photoionized through removal of a core C(1s) electron relax through single Auger decay. The resulting dications can then dissociate into several fragments. All ions and photoelectrons are guided to position and time sensitive multi-hit detectors with weak electric (7.5 V cm^{-1}) and magnetic (3.8 Gauss) fields [17]. The final positions and flight

times in fourfold (or fivefold) coincidence for each event are then used to determine the full vector momentum of each particle. The data were taken in event mode, and analysed offline.

The ions were detected with a two-layer square delay line anode with a 120 mm multi-channel plate pair [18]. Ions were accelerated by the electric field through a single 3.3 cm region before hitting the detector. Ion flight times were typically a few microseconds and multiple ions from a single photoionization event were easily distinguishable. The position and time of flight measurements of the ions allowed for determination of (1) the fragmentation channel, (2) the magnitude of the fragment momenta and therefore kinetic energy release of the dissociation, and (3) direction of the fragment momenta, which yields the orientation of the molecule for cases where fragments are ejected along bond axes. Ions up to 12 eV were collected with 4π solid angle.

The electrons were detected with a three-layer hexagonal delay line anode with a 80 mm multi-channel plate pair. The electrons were accelerated by the electric field through a 7.2 cm region followed by a 14.4 cm field free region before hitting the detector. This acceleration/drift geometry is the standard 2-1 time focusing condition, which improves the resolution along the field axis by compensating for the spatial width of the interaction region. The electrons, which are substantially less massive than the fragment ions were also confined by the magnetic field which was coaxial with the electric field. Electrons up to 6.5 eV were collected with 4π solid angle. Electrons of higher energy (such as the ejected Auger electron) with momentum vectors pointed directly toward the detector were also measured, albeit with substantially lower resolution.

The data were taken in list mode, and offline analysis allowed for a detailed differential study of the correlation between various parameters including ion fragmentation pathway, kinetic energy release, and the sets of fragment and electron momentum vectors associated with each event. MFPADs were constructed by transforming the electron momentum vector into the molecular frame when two bond axes were determined (three-fragment breakup, see section 4) and into the recoil frame when a single bond axis was determined (two-fragment breakup, see section 5). This procedure worked when the dissociation fragments were ejected along bond axes as described in section 4. However, this axial recoil approximation breaks down when the dynamics of the dissociation process removed the information of the initial molecule orientation from the measured fragment momenta, as demonstrated in section 5.

3. Complex Kohn variational calculations of MFPADS

The calculation of MFPADs for core-hole ionization requires a description of both the initial neutral electronic state of the molecule and the electron–ion scattering wavefunction for an electron scattering from the core-hole cationic state of the molecule. The well established complex Kohn variational method for electron–molecule scattering can be applied to electron scattering from molecular ions (including coupling between electronic states of the ion) and can thereby provide the final state wavefunction for such a calculation. The application of the complex Kohn method to photoionization has been described in some detail previously [19–21], and so we omit those details here.

The MFPAD for a fixed direction of the polarization vector is defined by the dipole matrix element in the equation

$$\frac{\mathrm{d}^2\sigma^{\Gamma_0}}{\mathrm{d}\Omega_{\hat{k}}\mathrm{d}\Omega_{\hat{\epsilon}}} = \frac{8\pi\omega}{3c}\left|\hat{\epsilon}\cdot\langle\Psi_0|\hat{\mu}|\Psi^-_{\Gamma_0,\vec{k}_{\Gamma_0}}\rangle\right|^2 \tag{3}$$

which defines the cross section for polarization $\hat{\epsilon}$ and ejected electron momentum $\vec{k}_{\Gamma_0}$ leaving the ion in state Γ_0. The target wavefunction for the electron–ion calculation is constructed as a single configuration using the natural orbitals from the averaged density matrices of the ion and neutral molecules, effectively applying what is known as 'Slater's transition state approximation' [22] for the photoionization process. The neutral initial state wavefunction, Ψ_0, is constructed as a single configuration from those natural orbitals. The complex Kohn scattering calculation then employs the static-exchange approximation with the target cation wavefunction constructed as a single configuration of the same natural orbitals, and completes the calculation of the final state $\Psi^-_{\Gamma_0,\vec{k}_{\Gamma_0}}$.

In this study we also measure and calculate the MFPAD in equation (3) integrated over polarization directions but with the molecule still in a fixed orientation. It is instructive to note the difference between the information contained in the two kinds of measurements, with $\hat{\epsilon}$ fixed or averaged over its orientations.

In terms of the cartesian components of the dipole operator we can write

$$I_{\vec{k}_{\Gamma_0}\hat{\epsilon}} = \hat{\epsilon}\cdot\langle\Psi_0|\hat{\mu}|\Psi^-_{\Gamma_0,\vec{k}_{\Gamma_0}}\rangle = \hat{\epsilon}\cdot\vec{M}_{\vec{k}_{\Gamma_0}}. \tag{4}$$

Integration over the directions of $\hat{\epsilon}$ then gives

$$\int\frac{\mathrm{d}^2\sigma^{\Gamma_0}}{\mathrm{d}\Omega_{\hat{k}}\mathrm{d}\Omega_{\hat{\epsilon}}}\mathrm{d}\Omega_{\hat{\epsilon}} = \frac{8\pi\omega}{3c}\frac{4\pi}{3}\left(|M^x_{\vec{k}_{\Gamma_0}}|^2 + |M^y_{\vec{k}_{\Gamma_0}}|^2 + |M^z_{\vec{k}_{\Gamma_0}}|^2\right) \tag{5}$$

and we see that while the three components of the transition dipole amplitude are combined coherently in equation (3) to produce a wide variety of shapes of the MFPAD for different polarization directions, the experiment that measures the MFPAD averaged over polarization directions measures an incoherent sum of the same three amplitudes.

In these studies we also calculated MFPADs averaged around one of the C_3 axes of the CH_4 molecule but with the polarization vector fixed at particular angles to that axis to compare with the measured RFPADs. These averages were accomplished by performing separate calculations of the MFPAD on grids of directions of electron momenta $\hat{k}$ for a set of orientations of the molecule and using Shepard interpolation [23] to evaluate the average. Those results will be used in section 5 for comparison with RFPADs measured in the $[CH_3^+, H^+]$ dissociation channel.

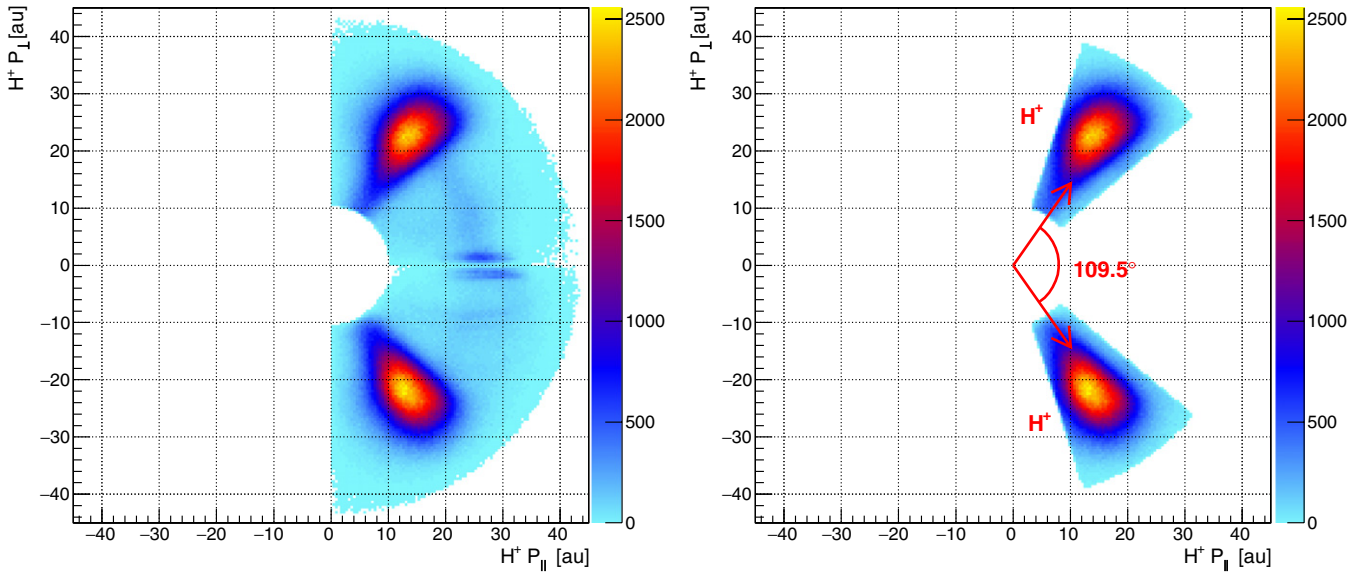

Figure 2. Ejected H^+ fragment momenta plotted in the frame defined by the vector components parallel and perpendicular to the momentum sum or C_2 axis of symmetry. Left: measured relative momenta of the H^+ fragments gated on kinetic energy release to isolate the $[H^+, H^+, CH_2]$ fragmentation channel. Right: the same with gates placed around the two 'islands' in order to discriminate signal from background.

4. High resolution MFPADs from observation of photoelectron in coincidence with two protons

One of the measured channels corresponded to the detection of two H^+ ions in coincidence without detecting the third fragment. The possible dissociation pathways that give rise to this are either (1) the $[H^+, H^+, CH_2^+]$ double-Auger channel where the third fragment wasn't detected or (2) the more probable $[H^+, H^+, CH_2]$ single-Auger channel where the neutral fragment is always lost. Figure 2 shows the momentum space distribution of the two hydrogen ions in the frame defined by their momentum sum. The horizontal and vertical axes correspond to the perpendicular and parallel components respectively. The data for the first hit on the detector is shown in the upper half of the figure, and the data for the second hit is shown on the lower half. There are clearly two islands separated by slightly more than the neutral ground state bond angle of 109.5°. We interpret this result to be due to ejection along the bond axes along with broadening of the angle due to the Coulomb repulsion of the two ions. In the right panel of figure 2 gates are set around the islands in order to discriminate against contaminant random events (background), but set broadly enough to include the locus of points where the island edges met the background.

Because of the high symmetry of CH_4, we were able to fully determine the orientation of the molecule with only these two vectors. This allowed the determination of the MFPADs shown in figures 3 and 4. These figures show the angular distribution in three dimensions by displaying intensity as both the radial coordinate and as a colour map range from weak or blue to strong or orange. In each case we present a comparison between the complex Kohn variational calculation and the experimental result, and in all cases, the agreement is excellent. The remaining discrepancy arises due to a combination of (1) the broad gating and binning of the statistics limited experimental data, (2) the quite complicated angular resolution of the measurement due to the variation of the momentum resolution through the momentum space and (3) the zero-point vibrational motion of the molecule. There is no clear way to unfold all of these, so we have chosen to present the theoretical and experimental results as they stand, which we consider sufficient for an insightful comparison.

Figure 3 shows the MFPAD at the lower photon energy where we have integrated over the polarization direction revealing only the contribution of the molecular potential to the electron angular distribution. If there were no influence of the molecular potential, then this distribution would be isotropic. However, we see here the striking result that for this photoelectron energy, the ejected electrons tend to emerge along the bond axes. The mechanism for this apparent focusing of the outgoing electron wave by the bonds is not fully understood at this time, but it has been predicted in two isoelectronic molecules, NH_3 and H_2O, by complex Kohn variational calculations like those presented here [21]. Since the wavelength of the ejected electron is more than five times the CH bond distance, this angular dependence must be understood as effects of electron–ion scattering rather than simple diffraction. Moreover, as we will see below this effect almost disappears at a photon energy only 10 eV higher. No simple model has yet produced even a semiquantitative representation of this behaviour.

Each column of panels in figure 4 corresponds to theory (top) and experiment (bottom) for the MFPADs arising from specific orientations of the molecule relative to the polarization axis. The left column corresponds to the polarization axis along the C_2 axis of symmetry, bisecting two hydrogen bond axes. In the middle column the polarization axis is perpendicular to a C_2 axis and constrained to the plane of two hydrogen bonds. In the right column the polarization axis is perpendicular to a C_3 axis and is in the plane with a carbon-hydrogen bond.

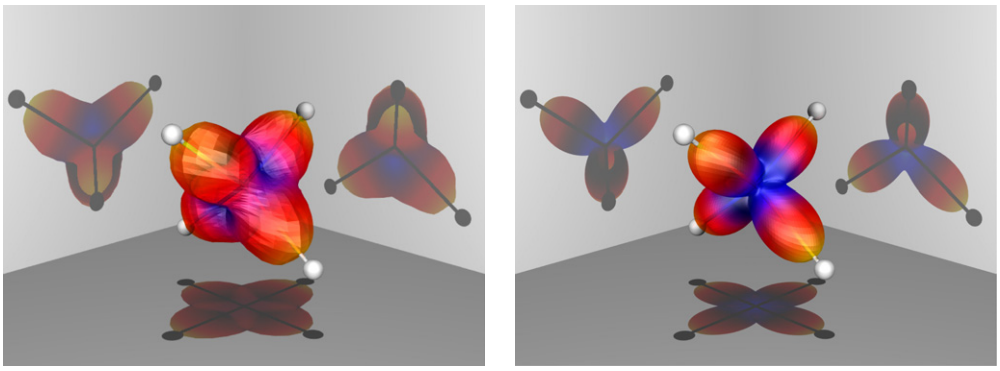

Figure 3. MFPAD for K-shell ionization with photon energy of 295 eV (electron kinetic energy of 4.25 ± 0.25 eV), in CH_4 observed (left) in coincidence measurement with $H^+ + H^+$ following Auger decay, and calculated (right) using the complex Kohn variational method. Data and theory are integrated over all orientations of the polarization vector.

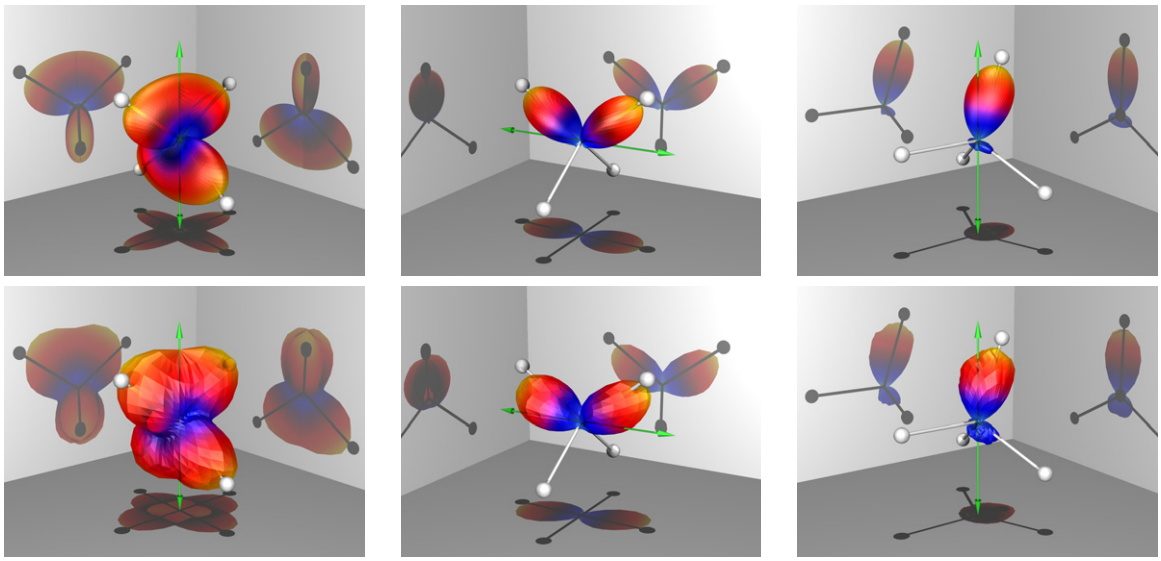

Figure 4. Theoretical (top row) and experimental (bottom row) MFPADs at a photon energy of 295 eV for particular orientations of the polarization axis in the molecular frame. The experimental data is for the $[H^+, H^+, CH_2]$ two-body channel. In the left column the polarization axis is aligned along a C_2 symmetry axis. In the middle column the polarization axis is perpendicular to the C_2 axis and constrained to the plane of two CH bonds. In the right column the polarization axis is perpendicular to the C_3 axis (a CH bond) but close to another CH bond.

An apparent competition of the tendency of the electron to be ejected along the polarization axis and its propensity to emerge along a bond direction can be observed in this figure. Even at this higher level of differentiation, we still find excellent qualitative agreement with the theoretical calculations, giving us confidence that we can use the calculations as a tool to elucidate fragmentation dynamics in more complicated dissociation pathways.

Figure 5 shows the MFPAD at a higher photon energy. The smaller cross section at these energies results in a dataset with limited statistics. Nonetheless the comparison between theory and experiment shows the same trend towards isotropy in the molecular frame at higher energies, as opposed to the lower energy results shown in figure 3. The calculated MFPAD shows six dimples along the C_2 axes (three in front and three at the back), which are also seen weakly in the experimental data. These details indicate that the two distributions likely match within the resolution of the observed MFPAD. More importantly, this comparison emphasizes the fact that the tendency of the ejected electron to emerge along a bond direction is observed over a limited energy range and has all but disappeared at this energy even though the wavelength of the electron is still nearly three times the CH bond distance. This behaviour has thus far proved quite difficult to model without a full scattering calculation like the Kohn calculations presented here.

5. The dynamics of dissociation into $H^+ + CH_3^+$ following Auger decay

5.1. Evidence for different dissociation mechanisms and dynamics at different kinetic energy releases

Another measured channel corresponds to the two-body fragmentation of the CH_4^{2+} dication into the $[CH_3^+, H^+]$ dissociation pathway. The momentum measurement of this channel only defines a single axis, so we are limited to comparing experiment to theory where we have integrated the calculation about the azimuthal angle relative to the broken bond axis. Doing so produced the surprising result found in

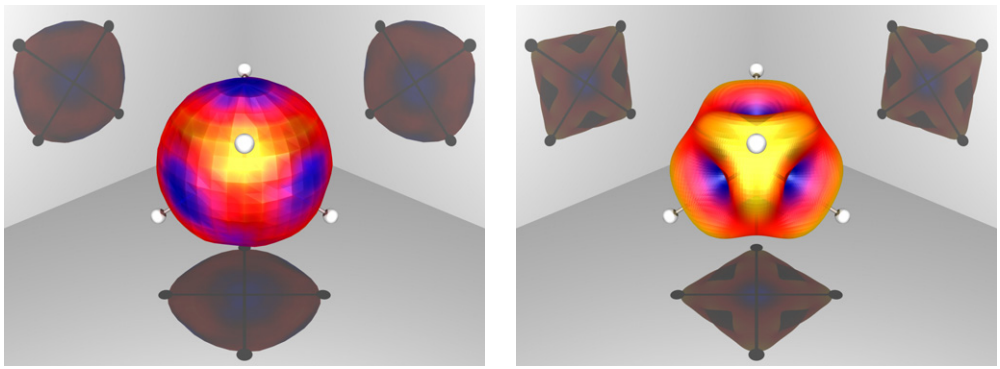

Figure 5. MFPADs integrated over all orientations of the polarization vector from measurement with photoelectron energy of 15.25 ± 0.25 eV (left) and from theoretical calculation with photoelectron energy of 15.24 eV (right). In each case the colour shading ranges from the minimum (blue) to maximum (yellow) of the angular distribution. Overall magnitude of the theoretical MFPAD is a factor of 1.8 smaller than the corresponding cross section in figure 4.

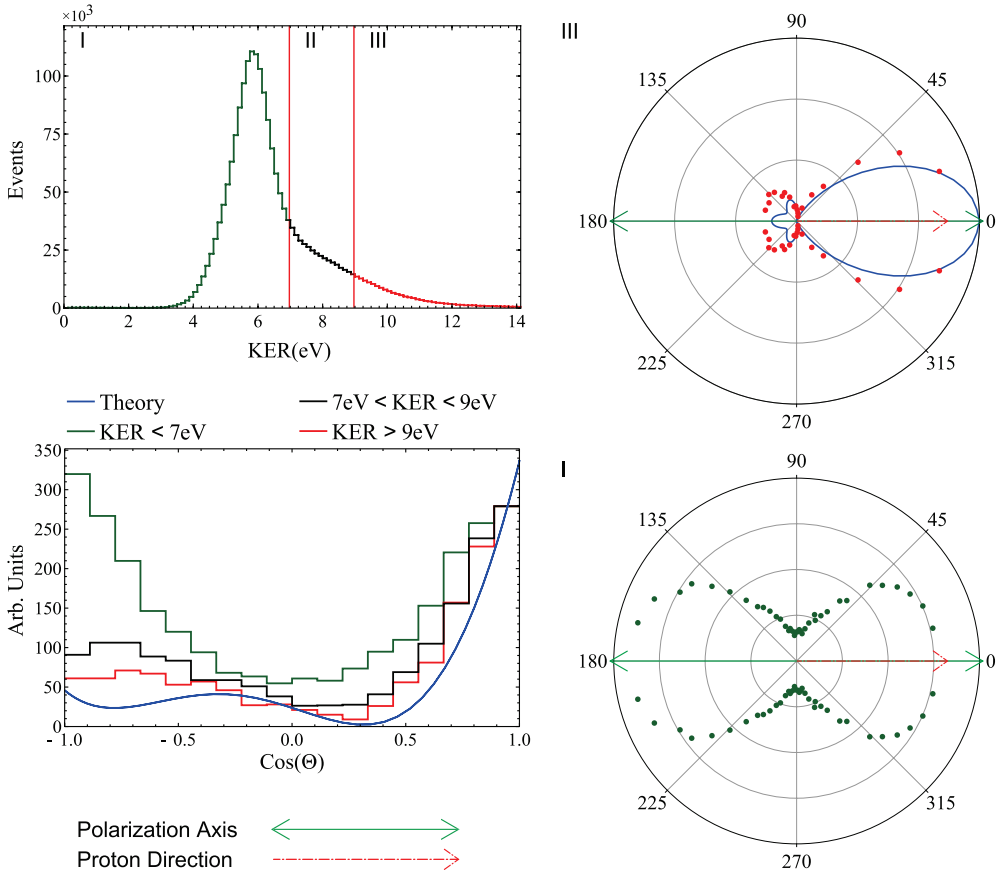

Figure 6. KER spectrum and RFPADs from measurements in the $[CH_3^+, H^+]$ channel at a photon energy of 295 eV with polarization along the recoil axis. The data are gated into three regions of KER: (I) less than 7 eV, (II) between 7 and 9 eV, and (III) above 9 eV. Using data for KER less than 7 eV produces the dipole-shaped RFPAD on the bottom right, indicating a severe breakdown of the axial recoil approximation, while the comparison with theory (solid line) shown in region III at top right shows closer agreement that indicates axial recoil behaviour at those energies. The RFPAD for all three KER regions, along with the theoretical RFPAD, are plotted in the bottom left panel.

figure 6, where RFPADs in the hydrogen recoil frame show an essentially dipole distribution for low KER but agree better with theory for high KER. We attribute this result to the contribution to this fragmentation channel from at least the two decay pathways described in section 5.2. If in one of the pathways (low KER) the molecule is distorted or the dication lives for a long time, then the direction of the ejected H^+ momentum will not correspond to the H bond axis. These observations lead us to the conclusion that the axial recoil approximation (in the sense of prompt dissociation along the bond being ruptured) appears to be valid for the high KER part of this channel but not for the sharper lower energy feature in the KER spectrum.

The theoretical RFPAD shown in figure 6 is calculated by averaging an MFPAD with the polarization along a CH bond around that bond axis (a C_3 axis). This calculation was done

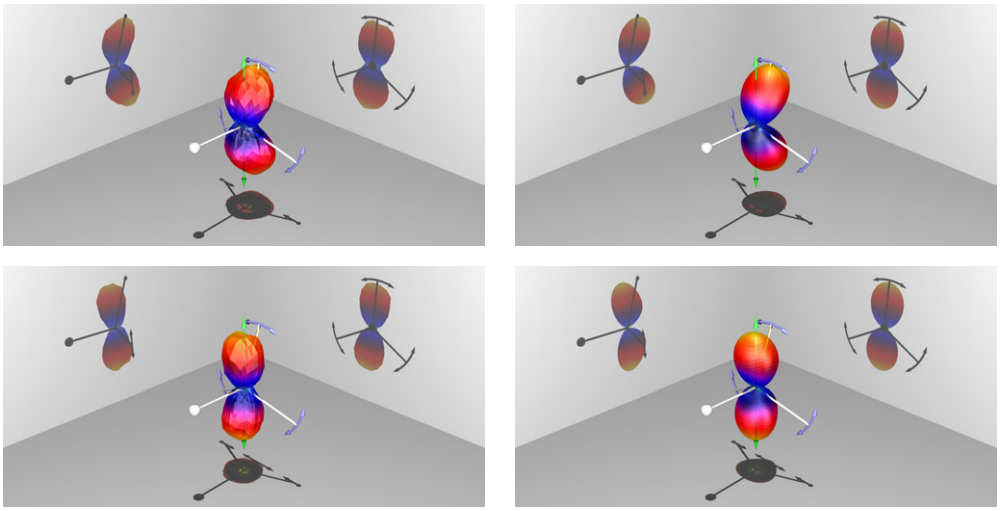

Figure 7. Experimental (left) and theoretical (right) RFPADs from complex Kohn variational calculations, averaged around a C_3 axis of methane. Top panels: 4.25 ± 0.25 eV photoelectron energy. Bottom panels: 15.25 ± 0.25 eV photoelectron energy. Both experimental RFPADs are generated from events that have a KER above 7 eV. Green arrows denote the direction of polarization. The orientation average was performed around the CH bond indicated by a line terminated with a sphere in each panel (the recoil axis), and thus the three hydrogens to the right were rotated around that bond to produce the averaged MFPADs (RFPADs) shown here.

with exactly the same amplitudes that appear in equation (4) and that were used to calculate the MFPADs compared with experiment in the $[CH_2, H^+, H^+]$ channel in figure 4. Thus the agreement at higher kinetic energies in the $[CH_3^+, H^+]$ channel is a strong indication of axial recoil dynamics that is supported by both theory and experiment. The question is: why does axial recoil apply only to the high KER portion of the process? The actual values of the KER are not enough to explain that trend since they are all greater than 4 eV where dissociation is far more rapid than the rotation of this molecule.

In figure 7 we show another, even stronger, indication that axial recoil dynamics are being observed at KERs above 7 eV. In that figure we compare the experimental RFPADs with the calculated ones for a polarization direction that is perpendicular to the recoil axis instead of along it. For both photon energies the agreement between the experimentally observed RFPAD and the one calculated by averaging the theoretical MFPAD around a C_3 axis is nearly perfect. That comparison leaves little doubt that the RFPADs measured in this channel are consistent with axial recoil and with the MFPADs measured in the $[H^+, H^+, CH_2^0]$ channel discussed earlier.

5.2. Electronic structure calculations and the identification of pathways to dissociation in states of CH_4^{++}

The RFPADs observed in the breakup leading to $[CH_3^+, H^+]$ shown in figures 6 and 7 immediately raise the questions: why does the axial recoil approximation evidently break down for KER values near the peak near 6 eV, while for higher KER values in the same arrangement the dissociation is apparently prompt and does satisfy axial recoil? And also, what states of the product CH_3^+ are being produced? To at least partially answer those questions we have performed calculations of portions of the potential surfaces for relevant states of the CH_4^{++} ion that can be produced by Auger decay.

Our point of departure is a result of Kukk *et al* [10]. By measuring the energies of Auger electrons in coincidence with the ionic fragments, these investigators were able to give compelling evidence in 2007 that the the CH_3^+ fragment originates from the ^{1}E state of CH_4^{++} in tetrahedral geometry and that the same state produces CD_3^+ from dissociation of CD_4^{++}. The C($1s^{-1}$) hole state of the molecule is created with a vibrational progression with only the symmetric stretch appreciably populated that has been observed to include the v = 0, 1 and 2 vibrational states [24, 25]. So we can assume that core photoionization and subsequent Auger decay occur in our experiments near the tetrahedral geometry of the neutral methane molecule.

In the tetrahedral (T_d) equilibrium geometry of neutral methane, far from the planar equilibrium geometry of the dication [26], the dominant electronic configuration of CH_4^{++} is $1a_1^2\ 2a_1^2\ 1t_2^4$. This configuration gives rise to four states with the term symbols $^3T_1$, ^{1}E, $^1T_2$ and $^1A_1$. Figure 8 shows the results of state-averaged multiconfiguration self-consistent field (MCSCF) calculations for a number of electronic states of the methane dication as one CH bond is stretched while the rest of the molecule remains in the equilibrium geometry of the neutral. The vertical line marks the point of T_d symmetry and the four dication states are labelled near to where they intersect that line. The details of these calculations are discussed in the appendix, so here we focus on the calculated potential curves and what they suggest about the dynamics of the dissociation of the methane dication.

When one C–H bond in CH_4^{++} is stretched, the symmetry of the molecule is reduced to C_{3v} and the nine individual spatial components corresponding to the $^3T_1$, ^{1}E, $^1T_2$ and $^1A_1$ states in T_d symmetry split into a $^3A_1$, a ^{3}E, two $^1A_1$ and two ^{1}E states in C_3v symmetry. Figure 8 shows that three of those states rise in energy as one CH bond is stretched and thus cannot, at least directly, dissociate into the $[CH_3^+, H^+]$ channel. The remaining three, of ^{1}E, ^{3}E and $^1A_1$ symmetry are dissociative.

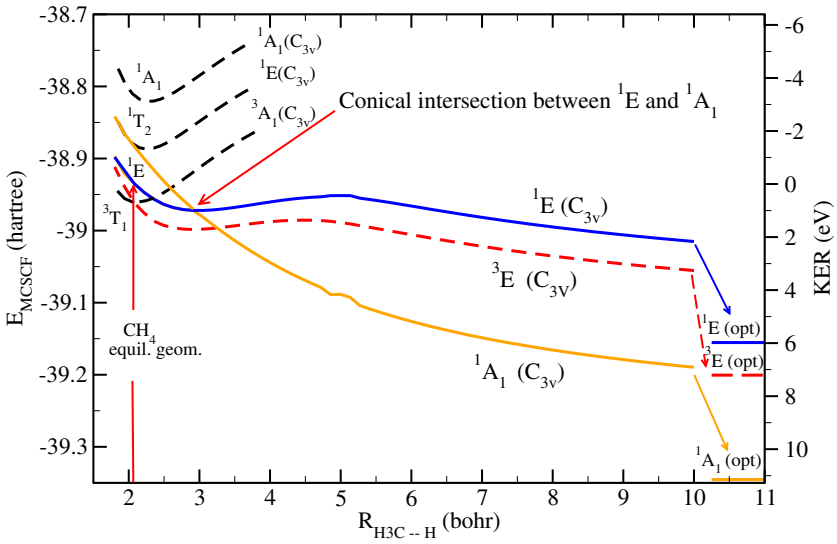

Figure 8. Potential energy curves from MCSCF calculations for the dissociation $CH_4^{++} \rightarrow CH_3^+ + H^+$ channel. Curves are with the CH_3^+ fragment fixed at the equilibrium geometry of methane. Asymptotes indicated by arrows are with CH_3^+ in the minimum energy geometry for each state. The kinetic energy release values on the right are for dissociation beginning on the ^{1}E state at the tetrahedral equilibrium geometry of neutral methane indicated by a red arrow.

We see from figure 8 that the ^{1}E state identified by Kukk *et al* [10] to be responsible for this dissociation can dissociate directly, by passing over the slight barrier in the calculated curves, but that it has a symmetry allowed crossing (conical intersection) with the $^1A_1$ state that is also dissociative. The dissociative curves in figure 8 are calculated with the CH_3^+ fragment frozen in the geometry of the neutral molecule so they are not limited to the lowest energy configurations of CH_3^+ in its ^{1}E, ^{3}E and $^1A_1$ states. Therefore to calculate the kinetic energy release predicted by this level of theory we require the energies of those minimum energy geometries. We therefore optimized the geometries of these states of the methyl cation as described in the appendix at the same level of MCSCF calculations (same active space) and in the same basis set used for the calculations on the dication, CH_4^{++}. Since both systems, CH_3^+ and CH_4^{++} have the same number of electrons, those calculations are therefore as nearly consistent with the ones producing the curves in figure 8 as is possible at the MCSCF level.

The ^{1}E and ^{3}E states are distorted by the Jahn–Teller effect, and the ground $^1A_1$ state of the methyl cation is planar. The optimized geometries are given in table 1. These states were also calculated by Flammini *et al* [12], but the geometries they found at an apparently different level of MCSCF were somewhat different. However that work did show that the asymptotic energies of these states compared with the energies of the corresponding states of CH_4^{++} in T_d symmetry suggested that there must be an intersection between the ^{1}E and $^1A_1$ states which is the one visible in figure 8.

The resulting values of the kinetic energy release for a dissociation beginning on the ^{1}E state of the dication are given in table 2. The energies of these states are lowered considerably by distortion into their optimum geometries. Those asymptotes are the ones that define our best estimate of the kinetic energy release from these calculations.

Table 1. Equilibrium geometries of states of the methyl cation from MCSCF calculations. For the E states, the lower of the components from Jahn–Teller splitting is given.

State	Geometry, symmetry	Angles	Bond distances (Å)
$^1A_1$	Planar, D_{3h} 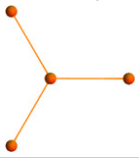	∠ HCH = 120°	R_{CH} = 1.095
^{3}E	Jahn–Teller, C_s 	∠ H′CH″ = 123.0° ∠ H″CH″ = 61.0°	$R_{CH'}$ = 1.092 $R_{CH''}$ = 1.193
^{1}E	Jahn–Teller, C_s 	∠ H′CH″ = 131.7° ∠ H″CH″ = 76.0°	$R_{CH'}$ = 1.090 $R_{CH''}$ = 1.204

Table 2. Kinetic energy release values from MCSCF calculations: Energy (^{1}E of CH_4^{++} in Td symmetry) - Energy (CH_3^+ optimized geometries in table 1).

State	KER from ^{1}E of CH_4^{++} (eV)
$^1A_1$	11.25
^{3}E	7.31
^{1}E	6.08

These KER values are consistent with the experimental observations in figure 6 if we identify the two processes contributing to this dissociation channel as

(i) ^{1}E of CH_4^{++} in T_d symmetry → conical intersection → the $^1A_1$ ground state of CH_3^+, with a maximum kinetic energy release of ≈11 eV.
(ii) ^{1}E of CH_4^{++} in T_d symmetry → directly to the lower component of the Jahn–Teller distorted state ^{1}E of CH_3^+, with maximum kinetic energy release of ≈6 eV.

The KER curve shown in figure 6 shows a peak at about 6 eV tailing off to lower KER, and these calculations identify that part of the spectrum with the ^{1}E state of the CH_3^+ fragment. The higher energy part of that KER spectrum can be identified with dissociation to the ground state of CH_3^+. Because that state is planar, far from the geometry of the CH_3 portion of methane in its initial tetrahedral geometry, it can be expected that the $^1A_1$ state of CH_3^+ is produced with high vibrational excitation, particularly in the out-of-plane bending modes.

The difference in the apparent MFPADs measured using the high and low KER portions of the spectrum separately is further evidence of the presence of two distinct dissociation pathways. Comparison with the theoretically calculated MFPAD, averaged over orientations of the CH_3^+ fragment around the dissociating CH bond direction, indicate that dissociation with high KER satisfies the axial recoil condition, while dissociation with lower KER in the 6 eV peak does not. That comparison is definitive, because the same amplitudes appearing in equations (3) and (5), which produce nearly perfect agreement between observed and calculated MFPADs from other channels, are the ones that produce these MFPADs averaged over CH_3^+ orientations.

While we can confidently assign the two regions of KER in figure 6 to these two mechanisms, we have not explored the complete nine-dimensional potential surfaces of the states involved to understand exactly why the dynamics of dissociation on the ^{1}E surface involves either significant distortion of the molecule away from the direct dissociation path, or even more complicated and longer lived dynamics. We can only say that the calculated barrier to dissociation for that state in figure 6 is only 0.45 eV starting from the equilibrium geometry of methane. Thus if Auger decay places the system wave packet at a range of different bond distances at least some of the initial wave packet for dissociation might be effectively below it. However, the path through the conical intersection to the $^1A_1$ state is calculated with considerable confidence to be steeply downhill to ground state products.

6. Conclusion

We have demonstrated that it is possible to produce fully three-dimensional molecular-frame photoelectron angular distributions (MFPADs) from a polyatomic molecule, and that when the dissociation dynamics follow axial recoil those MFPADs (or RFPADs) are consistent when measured in different dissociation channels. Complex Kohn calculations of these MFPADs, which are the same regardless of the channel for dissociation that happens after the photoionization event, can be used to distinguish channels where the dissociation follows axial recoil from those where it does not. Ultimately we anticipate that such calculations and measurements will become a valuable general tool for studying questions such as core-localization dynamics in larger symmetric molecules or the time-dependent measurements of conformation changes using attosecond pulses from next generation light sources.

Acknowledgments

This work was supported in part by the US Department of Energy Office of Basic Energy Sciences, Division of Chemical Sciences Contracts DE-AC02-05CH11231 and DE-FG02-10ER16146. CST acknowledges support from a California State University Maritime SoTL grant. Additional funding was provided by Deutsche Forschungsgemeinschaft and DAAD.

Appendix A. MCSCF calculations

The MCSCF calculations we report here were performed with the COLUMBUS 7.0 quantum chemistry code [27]. All the calculations we report were performed with the correlation consistent plus polarization triple zeta (cc-pvtz) basis sets for carbon and hydrogen. Complete active space (CAS) state-averaged MCSCF calculations were performed for the dissociative curves of CH_4^{++} shown in figure 8 that included all five components of the $^1A_1$, ^{1}E, and ^{3}E states. The $1a_1$ (≈ C 1s) orbital was held doubly occupied and the remaining six electrons were distributed in a CAS space of ten orbitals, giving a total of 2688 configurations in those calculations, which were performed in C_s symmetry so that the CAS space contained 7 a′ and 3 a″ molecular orbitals. The geometry of the CH_3 fragment was fixed in the tetrahedral geometry of methane with a CH bond distance of 2.05 bohr.

The other curves in that figure (in particular the black dashed curves that are not dissociative) are from similar state-averaged MCSCF calculations, but using all nine components of the $^3T_1$, ^{1}E, $^1T_2$ and $^1A_1$ states, which split as indicated in C_{3v} symmetry.

Geometry optimizations for the states of CH_3^+ were performed using the same CAS space of ten orbitals as follows: the energy of the $^1A_1$ state was minimized in an MCSCF with a single state using no symmetry, so that there were 4950 configurations in those calculations. The ^{3}E state geometry was optimized in state-averaged MCSCF calculations that included both Jahn–Teller components with 6930 configurations made from the same CAS space. The ^1E state is not the lowest singlet state, and so its geometry was optimized in state-averaged MCSCF calculations that included the lowest two singlets with 4950 configurations.

References

[1] Arasaki Y, Takatsuka K, Wang K and McKoy V 2010 *J. Chem. Phys.* **132** 124307
[2] Hockett P, Bisgaard C Z, Clarkin O J and Stolow A 2011 *Nature Phys.* **7** 612
[3] Williams J B *et al* 2012 *Phys. Rev. Lett.* **108** 233002
[4] Larsen J J, Hald K, Bjerre N, Stapelfeldt H and Seideman T 2000 *Phys. Rev. Lett.* **85** 2470
[5] Hansen J L *et al* 2011 *Phys. Rev.* A **83** 023406
[6] Landers A *et al* 2001 *Phys. Rev. Lett.* **87** 013002

[7] Yamazaki M, Adachi J, Teramoto T, Yagishita A, Stener M and Decleva P 2009 *J. Phys. B: At. Mol. Opt. Phys.* **42** 051001
[8] Dörner R, Mergel V, Jagutzki O, Spielberger L, Ullrich J, Moshammer R and Schmidt-Böcking H 2000 *Phys. Rep.* **330** 95
[9] Jahnke T, Weber Th, Osipov T, Landers A L, Jagutzki O, Schmidt L P H, Cock C L, Prior M H, Schmidt-Böcking H and Dörner R 2004 *J. Electron Spectrosc. Relat. Phenom.* **141** 229
[10] Kukk E *et al* 2007 *J. Phys. B: At. Mol. Opt. Phys.* **40** 3677
[11] Fainelli E, Alberti G, Flammini R, Maracci F, Bolognesi P, Mastropietro M and Avaldi L 2007 *J. Electron Spectrosc. Relat. Phenom.* **161** 51
[12] Flammini R, Satta M, Fainelli E, Alberti G, Maracci F and Avaldi L 2009 *New J. Phys.* **11** 083006
[13] Weber Th *et al* 2001 *J. Phys. B: At. Mol. Opt. Phys.* **34** 3669
[14] Ulrich B *et al* 2011 *J. Phys. Chem.* A **115** 6936
[15] Matsuda A, Takahasi E J and Hishikawa A 2007 *J. Chem. Phys.* **127** 114318
[16] Osipov T, Cocke C L, Prior M H, Landers A, Weber Th, Jagutzki O, Schmidt L, Schmidt-Böcking H and Dörner R 2003 *Phys. Rev. Lett.* **90** 233002
[17] Jagutzki O, Lapington J S, Worth L B C, Spillman U, Mergel V and Schmidt-Böcking H 2002 *Nucl. Instrum. Methods Phys. Res.* A **477** 256
[18] Jagutzki O *et al* 2002 *IEEE Trans. Nucl. Sci.* **49** 2477
[19] Rescigno T N, Lengsfield B H and Orel A E 1993 *J. Chem. Phys.* **99** 5097
[20] Miyabe S, McCurdy C W, Orel A E and Rescigno T N 2009 *Phys. Rev.* A **79** 053401
[21] Trevisan C S, McCurdy C W and Rescigno T N 2012 *J. Phys. B: At. Mol. Opt. Phys.* **45** 194002
[22] Slater J C 1974 *The Self-Consistent Field for Molecules and Solids: Quantum Theory of Molecules and Solids* vol 4 (New York: McGraw-Hill)
[23] Renka R J 1988 *ACM Trans. Math. Softw.* **14** 149
[24] Kukk E *et al* 2005 *Phys. Rev. Lett.* **95** 133001
[25] Püttner R, Arion T, Förstel M, Lischke T, Mucke M, Sekushin V, Kaindl G, Bradshaw A M and Hergenhahn U 2011 *Phys. Rev.* A **83** 043404
[26] Wong M H and Radom L 1989 *J. Am. Chem. Soc.* **111** 1155
[27] Lischka H *et al* 2012 COLUMBUS, an *ab initio* electronic structure program, release 7.0